NASA TECHNICAL MEMORANDUM

NASA TM X-73665

NASA TM X-73665

EXPERIMENTAL FATIGUE LIFE INVESTIGATION OF CYLINDRICAL THRUST CHAMBERS

by R. J. Quentmeyer
Lewis Research Center
Cleveland, Ohio 44135

TECHNICAL PAPER to be presented at the
Thirteenth Propulsion Conference
cosponsored by the American Institute of Aeronautics
and Astronautics and the Society of Automotive Engineers
Orlando, Florida, July 11-13, 1977

EXPERIMENTAL FATIGUE LIFE INVESTIGATION OF CYLINDRICAL THRUST CHAMBERS

R. J. Quentmeyer
National Aeronautics and Space Administration
Lewis Research Center
Cleveland, Ohio

E-9188

Abstract

During a test program to investigate low-cycle thermal fatigue, 21 of 22 cylindrical test sections of a cylindrical rocket thrust chamber were thermally cycled to failure. Cylinder liners were fabricated from OFHC copper, Amzirc, and NARloy-Z. The cylinders were fabricated by milling cooling channels into the liner and closing out the backside with electrodeposited copper. The tests were conducted at a chamber pressure of 4.14 MN/m^2 (600 psia) and an oxidant-fuel ratio of 6.0 using hydrogen-oxygen as propellants. The average throat heat flux was 54 MW/m^2 (33 $Btu/in^2/sec$). All of the failures were characterized by a thinning of the cooling channel wall and eventual failure by tensile rupture. The 1/2-hard Amzirc material showed little improvement in cyclic life when compared with OFHC copper; while the NARloy-Z and aged Amzirc materials had the best cyclic life characteristics. One OFHC copper cylinder was thermally cycled 2044 times at a steady-state hot-gas-side wall temperature of 514 K (925° R) without failing. The cycles to failure data could be correlated with either hot-gas-side wall temperature, or hot-gas-side to backside wall temperature difference. However, the cyclic life characteristics based on temperature do not agree with the published results of uniaxial, isothermal strain tests.

Introduction

The Space Shuttle vehicle has introducted a new era in rocket engine design with its unique set of requirements for high performance, reusability, light weight, and compact size. To meet these requirements, rocket engines must be designed to operate at elevated pressure levels and must utilize thrust chamber materials and fabrication techniques capable of withstanding large numbers of thermal cycles, high heat flux levels and high strain levels.

The Space Shuttle Main Engine (SSME) operates at a chamber pressure of 20.7 MN/m^2 (3000 psia), has a throat heat flux of 131-147 MW/m^2 (80-90 $Btu/in^2/sec$), and a life requirement of 55 thermal cycles. Beyond the SSME, the thrust chambers for an Orbit Transfer Vehicle (OTV) propulsion system may have a life requirement of 200-300 thermal cycles, as well as the requirements for high performance, light weight and small size.

Presently, thrust chamber life is limited by low cycle thermal fatigue, induced by high strain levels which cause cracks in the hot-gas-side wall. To meet these design requirements, reusable regeneratively-cooled thrust chambers having high throat heat flux levels must utilize materials having high thermal conductivity, such as copper or copper alloys. This allows a wall thickness sufficient to carry the cooling pressure and thrust loads, while maintaining reasonable wall temperatures and coolant pressure drop. Until recently, very little low cycle thermal fatigue data existed for this class of materials.

In 1967, low cycle fatigue was observed in a milled channel thrust chamber fabricated from copper[1, 2]. Additional thrust chamber cyclic testing was later reported in Refs. 3 and 4. Most of that thrust chamber work involved the use of three materials: oxygen-free, high conductivity (OFHC) copper; Amzirc, a copper-zirconium alloy developed by American Metal Climax, Inc.; and NARloy-Z, a copper-zirconium-silver alloy developed by Rocketdyne, a division of Rockwell International. In all of that work, only one or two thrust chambers were fabricated from each material, thus limiting the data base. In addition to the low cycle fatigue work being done with rocket thrust chambers, another investigator inserted water-cooled Amzirc tubes through the combustion zone of a rocket thrust chamber to study the effect of a rocket combustion environment on the material[5]. In addition to the rocket chamber tests, isothermal low cycle fatigue tests were performed on specimens of 12 different copper base alloys which were candidate materials for thrust chamber fabrication[6]. Hannum et al[7] attempted to extend the data base by testing a total of 13 thrust chambers fabricated from OFHC copper and Amzirc. They attempted to correlate the experimental life results with analytical life predictions using the uniaxial, isothermal cyclic test data of Ref. 6 and the materials properties data of Ref. 8. For the most part, the attempt to correlate the experimental life data with the analytical life predictions was unsuccessful. It was suggested that the failure mechanism was not pure low cycle thermal fatigue that had been presupposed and upon which the life predictions were based.

In most of the work, the investigators concluded that the failures were premature, i.e. the material failed sooner than was expected when compared with the uniaxial, isothermal fatigue tests performed in a laboratory, such as the results reported in Ref. 6. The premature failures were attributed to flaws in the material, improperly processed material, machining flaws, and hot spots.

In light of this, an experimental investigation was initiated at the Lewis Research Center to conduct additional low cycle fatigue tests in rocket thrust chambers. The purpose of the work was to test a sufficient number of thrust chambers to get better understanding of the failure mechanism, determine the effects of wall temperature on cyclic life, and to rank the material life characteristics for comparison with the isothermal tests of Ref. 6.

A different and unique approach was taken in the design and fabrication of the thrust chambers used in this work. An annular combustion chamber configuration was used, consisting of an annular injector, a liquid hydrogen cooled outer cylinder, which served as the test section, and a contoured water cooled centerbody which formed the throat.

STAR Category 20

The advantages of this configuration, which is shown in Fig. 1, were its simplicity, low cost, and ability to provide a higher throat heat flux for a given chamber pressure and throat inside diameter. Twenty-two cylinders were fabricated by milling cooling channels into liners fabricated from the material to be evaluated. The channels were closed out by electrodepositing copper to the backside. Three materials were chosen for the liners: OFHC copper, Amzirc, and NARloy-Z. These materials were chosen because all of them have been considered, or are now being used, as thrust chamber materials and the majority of the experimental work on advanced thrust chamber design has been done with these materials. The cylinders were cyclically tested until failure occurred due to fatigue cracks in the hot-gas-side wall. After each failure, a post destructive analysis was performed on the cylinder. The results of the destructive analysis and the effect of wall temperature on cyclic life is presented.

Apparatus

Cylindrical Thrust Chamber Assembly

Figure 1 shows a schematic of the cylindrical thrust chamber assembly. The thrust chamber consisted of an annular injector, a liquid hydrogen-cooled outer cylinder, which served as the test section, and a water-cooled centerbody, which formed the annular thrust chamber throat. The thrust chamber had a contraction and expansion area ratio of 1.79. At a chamber pressure of 4.14 MN/m^2 (600 psia) the thrust was approximately 5.34 kN (1200 lbf) and produced an average throat heat flux of 54 MW/m^2 (33 $Btu/in^2/sec$). Gaseous hydrogen and liquid oxygen were used as propellants. The cylindrical test section was separately cooled with liquid hydrogen, which was disposed of by a burn-off stack. The cooling water for the centerbody was dumped at the thrust chamber exit.

Cylindrical Test Section

The cylindrical test sections were made in two lengths, 10.16 cm (4.0 in.) and 15.24 cm (6.0. in.), and had an inside diameter of 6.60 cm (2.6 in.). Table 1 shows the cylinder configurations. Twelve cylinder liners were fabricated from OFHC copper, seven from Amzirc, and three from NARloy-Z. The Amzirc was approximately 99.85% copper and 0.15% zirconium. The NARloy-Z was approximately 96.5% copper, 3.0% silver, and 0.5% zirconium.

The copper liners were machined from forged billets with no special heat treatment. The Amzirc liners were hot spun from "pancake" forgings and then cold spun to a 1/2-hard condition. One Amzirc liner was aged at 482° C (900° F) for four hours. The NARloy-Z liners were hot spun, solution annealed and aged. Figure 2 shows a cross-section of the cylinder wall with the cooling channel dimensions and instrumentation locations. Seventy-two constant area cooling channels, 0.169 cm (0.0665 in.) wide and 0.127 cm (0.05 in.) high, were machined into the liner billets. The cooling channel wall was 0.089 cm (0.035 in.) thick and the ribs were 0.127 cm (0.05 in.) wide. After machining, the cooling channels were filled with wax and a copper closeout electrodeposited to the backside. The wax was then melted out of the cooling channels and the manifolds added. The cylinders were designed to be separately cooled with liquid hydrogen at a nominal flow rate of 0.91 Kg/sec (2.0 lbm/sec).

Instrumentation

The instrumentation consisted primarily of chromel/constantan backside wall and rib thermocouples. The backside wall thermocouples were located at four circumferential locations 90° apart at the throat plane. There were two additional backside thermocouples, one 1.49 cm (0.586 in.) upstream of the throat plane and one 1.27 cm (0.50 in.) downstream of the throat plane. The junctions of the backside thermcouples were peened into small holes drilled into the backside surface. Four rib thermocouples were located at the throat plane of each cylinder. Two thermocouples were located 0.089 cm (0.035 in.) from the hot-gas-side wall, and two were located 0.178 cm (0.070 in.) from the hot-gas-side wall. Details of the thermocouple locations are shown in Fig. 2. The rib thermocouples were the same as those described in Ref. 7. Each thermocouple consisted of a chromel and constantan wire 0.025 mm (0.001 in.) in diameter inside a sheath made of 0.356 mm (0.014 in.) stainless steel tubing. The junction was made in a ball of silver solder which was plated with 0.005 mm (0.0002 in.) of gold. The probe was then spring loaded against the bottom of the rib hole. Three of the cylinders had eight additional rib thermocouples, four located 1.49 cm (0.586 in.) upstream and four located 1.27 cm (0.50 in.) downstream of the throat plane to obtain an axial thermal profile. Figure 3 shows a 10.16 cm (4.0 in.) cylinder on which six backside and twelve rib thermocouples had been installed. The liquid hydrogen inlet temperature was measured by a platinum resistance bridge transducer inserted in the inlet manifold. The hydrogen outlet temperature was measured by a chromel/constantan thermocouple inserted in the outlet manifold.

Injector

Figure 4 shows the thrust chamber injector. Gaseous hydrogen and liquid oxygen were used as propellants. Liquid oxygen was injected through 70 showerhead tubes arranged in two circular rows, 36 in the inner row and 34 in the outer row. The tubes were made of 0.23 cm (0.091 in.) O.D. stainless steel having a 0.03 cm (0.012 in.) thick wall. Two chamber pressure taps were located in the outer row of oxidizer tubes. The gaseous hydrogen was injected entirely through the porous Rigimesh face plate. The face plate was made removeable, so that it could be replaced if damaged. Injector uniformity tests were performed with ablative chambers and the uniformity was found to be satisfactory. Characteristic exhaust velocity efficiency ranged from 93-96%.

Centerbody

Figure 5 shows the thrust chamber centerbody. The centerbody was fabricated by machining 40 rectangular cooling channels into the outer periphery of a contoured Amzirc forging. The cooling channels were closed out by electrodepositing copper to the outer surface and then machining to the final contour. The centerbody had a 4.06 cm (1.6 in.) O.D. in the combustion zone and a 5.33 cm (2.1 in.) O.D. at the throat. The expansion half-angle was

7.5°. The centerbodies were made in two different lengths to accommodate the 10.16 cm (4.0 in.) and 15.24 cm (6.0 in.) length cylinders. The centerbody was inserted through the center of the injector and bolted into place from the back side.

Since the centerbody had to endure the same heat load as the cylindrical test section, a 0.076 - 0.127 mm (0.003 - 0.005 in.) zirconium-oxide flame sprayed coating was applied to the wall to reduce the heat load and prolong the centerbody life. Every 100-200 cycles, the centerbody was removed to replace the coating that had eroded or spalled off. After 1000-2000 cycles, the centerbody had to be replaced due to failure by low cycle fatigue. The centerbody was cooled with a nominal water flow of 5.44 Kg/sec (12 lbm/sec). The water entered the centerbody behind the injector, passed through the cooling channels and was dumped at the thrust chamber exit.

Test Facility

The tests were conducted at the Lewis Research Center rocket engine test facility. This is a 222,410 Newton (50,000 lbf) sea-level rocket test stand equipped with an exhaust-gas muffler and scrubber. The facility used pressurized propellant storage tanks to supply the propellants to the thrust chamber. The propellants were liquid oxygen and ambient temperature gaseous hydrogen. Liquid hydrogen was used to cool the cylindrical test section and water was used to cool the centerbody. Figure 6 is a schematic of the test facility showing the propellant and coolant supplies and the instrumentation. The liquid hydrogen used to cool the cylinder was disposed of through a burn-off stack. The thrust chamber exhaust gas and the centerbody water coolant were expelled into the scrubber. Due to the small volume of the thrust chamber combustion zone, an external igniter was used to back-light the combustion chamber. The igniter used gaseous oxygen and gaseous hydrogen as propellants. The ignition source was a high voltage spark.

Data Recording

All pressures and temperatures were recorded in digital form on a magnetic tape for entry into a digital computer. The digital recording system was set at a basic sampling rate of 2500 words per second. After processing, all of the data, and calculations performed on the data, could be printed out on the control room terminal at 0.1 second intervals.

Test Procedure

The cycle chosen for the tests was one where the heat-up portion of the cycle was long enough for the hot-gas-side wall temperature to reach steady-state, and where the cool-down portion of the cycle was long enough to bring the entire cylinder back to liquid hydrogen temperature. The cycle to achieve this condition was 3.5 seconds in duration, 1.7 seconds from ignition to the end of the combustion portion of the cycle, and 1.8 seconds to bring the cylinder back to liquid hydrogen temperature. The liquid hydrogen coolant was continuously flowed throughout a cyclic test, however, the weight flow varied from its initial rate as a function of the heat load to the cylindrical test section. Figure 7 is a display from a computer plotting routine of chamber pressure and liquid hydrogen-coolant weight flow showing how the liquid hydrogen weight flow varied with the heating cycle. During the first cycle of any given test a liquid hydrogen precool was used to bring the entire cylinder to liquid hydrogen temperature before ignition of the thrust chamber propellants. Short tests, consisting of just two cycles, were made with each new cylinder to establish the desired rib temperature condition. The liquid hydrogen coolant weight flow was varied to obtain the desired rib temperature. After the desired test conditions were achieved, the thrust chamber was continuously cycled until the supply of liquid hydrogen was nearly depleted. Generally, 70-90 cycles could be achieved on one tank of liquid hydrogen.

A solid state timer, accurate and repeatable to ±0.0001 second was used to program the test events. Fuel and oxidizer flows were controlled by initially setting fixed valve positions which would nominally set chamber pressure and mixture ratio. After the nominal chamber pressure was reached, both chamber pressure and mixture ratio were adjusted to the desired condition by a controller. The liquid hydrogen coolant weight flow and pressure were set by a combination of tank pressure, and upstream and downstream valve positions. The centerbody water flow was set to its maximum rate by pressurizing the water tank to a pressure of 10.34 MN/m^2 (1500 psia).

The tests were monitored by a closed-circuit television camera and a test cell microphone. The TV and audio outputs were recorded on magnetic tape for playback. The cylinder was assumed to have failed when the first through the wall crack had developed. The failure could be detected by both audio and visual means. When the wall developed a through crack, a sudden and distinct high pitch hissing sound could be heard and a vapor streak could be seen skewed to one side of the thrust chamber exhaust during the chill-down, or engine off, portion of the cycle. When this was detected, the cyclic testing was terminated. When the TV-audio tape was played back, the exact cycle during which the failure occurred could be determined. Figure 8 shows the cylindrical thrust chamber during the combustion portion of a cyclic test.

Test Results

Twenty-one of the 22 cylinders fabricated for this program were thermally cycled to failure. Twelve of the cylinders had liners fabricated from OFHC copper, three from NARloy-Z, six from Amzirc in the 1/2-hard condition, and one Amzirc liner which was aged. All but three of the cylinders were instrumented with backside wall and throat rib thermocouples. Table I shows the cylindrical test section configurations and the cycles to failure test results. In all cases, the failure occurred at the thrust chamber throat plane, which was the location of maximum heat flux.

Post Test Destructive Analysis

After failure, each cylinder was subjected to post test destructive analysis. The cylinders were sectioned in the region of failure and photographed.

A segment of the cylinder wall cross-section was etched at the location of failure and micrographs were made that showed changes in grain structure from the rib base to the crack location in the cooling channel wall.

Figure 9 shows the fatigue crack in the throat region of OFHC copper cylinder S/N 33, which failed after 220 cycles. The crack is approximately 0.51 cm (0.20 in.) long and is typical of the fatigue failures. Note the roughing, or "orange peel" appearance of the wall. This effect was more prevalent in the OFHC copper cylinders than in either the Amzirc or NARloy-Z cylinders. Figure 10 shows a cross-section of S/N 33, 0.15 cm (0.60 in.) downstream of the crack location. Also shown in the figure is a schematic of the wall section as it would have appeared prior to the cyclic testing. It can be seen that every cooling channel has deformed to some degree. The deformation varies all the way from an arched, or outward bulging appearance of the cooling channel wall toward the cylinder centerline to, in the most severely deformed channels, a "doghouse" shape. An arrow shows the channel in which the failure occurred. There was no one particular circumferential region in which the failures occurred. In the 21 cylinders cycled to failure, the cracks occurred at random circumferential locations.

Figure 11 shows the cooling channel wall failure of cylinder S/N 44 which had a 1/2-hard Amzirc liner. Also, the layers of the electrodeposited copper closeout can be seen in this figure. The failure is characterized by a thinning of the cooling channel wall at the centerline, which can readily be seen in the cooling channels adjacent to the failed channel. The bulging of the channel walls toward the cylinder centerline and the "doghouse" shape of the deformed channels is pronounced. All of the failures, regardless of the liner material, were characterized by a thinning of the cooling channel wall at the centerline. This type of failure was also typical of the failures reported in Refs. 1, 4, and 7.

Figure 12 shows an etched cross-section of the failed cooling channel wall in cylinder S/N 10, which had a NARloy-Z liner. Here again, the thinning of the wall and the deformation of the cooling channel to the "doghouse" shape is characteristic of the failure. Roughening of the hot-gas-side wall was also typical of the failures. Note the change in the grain size from the base of the rib to the crack region of the wall. The smaller grains in the crack region indicate a recrystallization without accompanying grain growth. Microphotographs indicated that some degree of recrystallization had occurred in the crack region on every cylinder, regardless of the liner material. In all cases, the grain size in the crack region was smaller than the grains in the undeformed rib, showing the effects of the plastic deformation. Hardness readings indicated that the OFHC copper and Amzirc strain softened in the region of the crack, whereas the NARloy-Z either retained its hardness or strain hardened in the region of the crack. This agrees with the results of the isothermal tests reported in Ref. 6.

The mechanism that produces the progressive thinning and eventual failure of the cooling channel wall is still conjectural. Hannum et al[7] attributed the failures to creep rupture and perhaps thermal racheting. Rocketdyne described the wall failure in a post test analysis of a NARloy-Z, SSME subscale chamber as being caused by strain induced creep, or cyclic strain induced deformation, to differentiate between a classical creep mechanism and the failure mechanisms encountered in these types of thrust chambers. The process that causes eventual failure is probably due to a combination of many things and the following is a hypothesis of the chain of events.

During each heating cycle, there exists a large temperature difference between the hot inner wall and the relatively cool outer jacket of the thrust chamber. The hot inner wall tries to expand but is constrained by the cool outer jacket. Therefore, a large thermal compressive strain is induced in the hot inner wall causing it to plastically deform in all three orthogonal planes. After several cycles the channel wall starts to bulge outward toward the thrust chamber centerline. This probably is due to the biased pressure load in the cooling channels, which is always higher than the combustion chamber pressure, and the fact that the hot-gas-side of the wall goes plastic first during the transient start-up. Thermal analysis also indicates that the hot-gas-side wall temperature is higher at the midpoint of the cooling channel than at the midpoint of the rib, and thus the coolant channel midpoint is the weakest point on the wall surface. During the chilldown portion of the cycle, the reverse takes place and the hot-gas wall goes into tension. The strain is not completely reversed because there is not a sufficient load component to push the wall back to its original position. Therefore, a net outward deformation results with each cycle. As the cyclic loading continues, the wall starts to thin in much the same way as a test specimen necks down during a cyclic tensile test in which the material goes above the yield stress during each cycle. After extensive deformation of the wall, the strain level is increased by a hypothesized increase in the wall temperature due to two processes. First, the cooling channel cross-sectional area increases and the coolant-side heat transfer coefficient is thereby reduced due to a lower mass flux in the region. Second, the outward deformation causes the hot-gas-side heat transfer coefficient to increase due to a roughening of the wall that accompanies the deformation. Both of these effects combine to increase the wall temperature in the deformed region and accelerate the failure mechanism. The failure eventually occurs when the cooling channel wall thins to the point that it fails by tensile rupture.

Post Test Thermal Analysis

One of the objectives of this program was to determine whether the cyclic life could be correlated with the hot-gas-side wall temperature. Since hot-gas-side wall temperature was not a measured parameter, the temperature had to be extrapolated from the measured rib and backside wall temperatures by the use of a thermal analysis.

Due to the large amount of data obtained in the experimental testing, a detailed analysis using the data from every cycle was not possible. However, random samples of all of the measured parameters were taken throughout the life of each cylinder. Analysis of the data confirmed that once the desired cycle was established for a given cylinder, the test parameters remained essentially the same throughout

the life of the cylinder, or until severe distortion of the cylinder wall had occurred. Thus, it was concluded that any cycle was representative of a "nominal" cycle throughout the cylinder life.

A further analysis was conducted to determine the circumferential variation in the wall temperature that occurred due to injector streaking and/or mislocation of the rib thermocouples. The analysis revealed that the average circumferential variation in the steady-state rib temperatures for all of the cylinders tested was ±21° C (70° F). Also, inspection of all of the failed cylinders showed that the cracks occurred in random circumferential locations, and not necessarily in the region of the hottest rib thermocouple temperature. None of the cracks occurred at an exact rib thermocouple location. Therefore, once the selected or "nominal" cycle was chosen for analysis, the temperatures from the rib thermocouples located 0.089 cm (0.035 in.) from the hot-gas-side wall were averaged. In like manner the temperatures from the rib thermocouples located 0.178 cm (0.070 in.) in depth were averaged, and the temperatures from the four backside thermocouples were averaged. Although some of the cylinders had thermocouples at other axial locations, only the data from the throat plane thermocouples were used in this analysis.

The next procedure was to develop a thermal model of the cylinder wall, and with the use of a thermal analyzer program and the experimental temperature data, calculate a pseudoexperimental hot-gas-side wall temperature. Figure 13 shows the model that was developed to perform the thermal analysis. Due to symmetry, only one-half of a cooling channel wall cross-section was required for the model. The representative wall cross-section was divided into 35 elements with a temperature node at the center of each element. There were surface nodes on each of the elements along the model boundaries, however, they are not shown on the figure. The relative locations of the thermocouples used to collect the experimental temperature data are also indicated in the Fig. 13.

The thermal analyzer program used to generate the cross-sectional wall temperature profile was the SINDA[9] program. Input to the SINDA program requires the hot-gas-side and coolant-side boundary conditions as a function of time, so that a temperature profile can be generated as a function of time. The steady-state hot-gas-side heat transfer coefficient was obtained from unreported data using a calorimeter with the cylindrical thrust chamber configuration. The steady-state coolant side heat transfer coefficient was calculated from empirical correlations which best describe convective heat transfer to liquid hydrogen. In addition, the coolant-side heat transfer coefficient was varied around the cooling channel periphery to reflect the variation due to the different wall temperatures that exist around the periphery. The hot-gas-side and the coolant-side heat transfer coefficients during the transients were not available from experimental data, therefore, as an initial input, they were assumed to vary from their steady-state values in proportion to variations in chamber pressure and liquid hydrogen weight flow for each time slice. Plots such as shown in Fig. 7 were used to make the adjustments in the heat transfer coefficients. This procedure did a reasonable job of fitting the thermocouple data, although minor adjustments were made in the boundary conditions, where needed, to best fit the data. The SINDA program is capable of performing a three dimensional thermal analysis, but only a two-dimensional analysis, at the throat plane of the thrust chamber was used for this work.

Figure 14 shows the matching of the thermal analysis with the experimental data of the 190th cycle of Amzirc cylinder S/N 40 using the SINDA thermal analyzer. The program outputs the temperature for each nodal point in the model, however, in this figure only the matching of the thermocouple data and the projected hot-gas-side wall temperature of element 1 is shown. Element 1 is presented because the maximum hot-gas-side wall temperature occurs at the cooling channel center. Using this technique, a cross-sectional temperature profile as a function of time could be generated for each cylinder. The hot-gas-side wall temperature obtained in this manner was probably not the maximum wall temperature that occurred at the crack location, due to the phenomenon described in the Post Destructive Analysis section, but rather, was representative of the nominal hot-gas-side wall temperature that existed throughout the cyclic testing of a given cylinder.

It was assumed that the best projected hot-gas-side wall temperature was obtained when the calculated temperature data matched the experimental data of the thermocouple closest to the hot-gas wall. When this was done, a perfect match of the thermocouple data at the other two locations could not necessarily be achieved, as seen on Fig. 14. This was probably due to axial conduction effects not accounted for in this two-dimensional analysis.

Using the procedure outlined above, the steady-state hot-gas-side wall temperature was calculated for each cylinder and plotted as a function of cycles to failure. Figs. 15 and 16 show the results for the OFHC copper and 1/2-hard Amzirc data, respectively. The solid symbol data point shown on Fig. 15 is for OFHC copper cylinder S/N 48. This cylinder was cycled 2044 times at a hot-gas-side wall temperature of 514 K (925° R) and still had not failed when the tests were terminated. The wall in the throat region was just beginning to roughen and, even though the number of cycles to failure was not determined, the data point was used in the curve fit, as the slope of the curve would not have changed significantly even if the cylinder had lasted 3000 cycles. The only other data point between 236 and 2044 cycles was for cylinder S/N 1 which failed at 817 cycles. There were no instruments on that cylinder, and therefore, the data point does not appear on the figure. It was found that a good correlation of the data resulted using a straight line when the data was plotted on log-log paper. The equations for the curve fits are shown on the figures.

In Fig. 17 the data points for the half-hard Amzirc and OFHC copper of Figs. 15 and 16 are combined. Although, the Amzirc line falls slightly above the OFHC copper line, it would appear that one line would adequately fit the data, which would imply that the 1/2-hard Amzirc is no better than the pure copper in terms of thrust chamber life. This was found to be the case for the Amzirc and OFHC copper thrust chamber tests reported in Ref. 7. They concluded that the Amzirc used for the thrust chamber fabrication was not the same as that used in the laboratory tests reported in Ref. 6. The test results reported in Ref. 6 showed that the

cycle life of 1/2-hard Amzirc was far superior to OFHC copper. However, it should be pointed out that the comparison made here is based on the hot-gas-side wall temperature, whereas the comparison made in Ref. 6 is based on strain range.

Three other data points are shown on Fig. 17, but not included in the curve fits. The half-solid diamond shaped symbol is for an Amzirc cylinder in which the liner was first cold spun to the 1/2-hard condition and then aged at 482° C (900° F) for four hours. The solid triangle symbols are for the cylinders having NARloy-Z liners, which had been hot spun, solution annealed and then aged. There was a third NARloy-Z cylinder which failed at 679 cycles and appears in Table I. However, there were no instruments on that cylinder and thus no projected hot-gas-side wall temperature. Although the data are limited, at a given temperature, the NARloy-Z and aged Amzirc materials show an improvement in cyclic life over the OFHC copper and 1/2-hard Amzirc materials.

A conventional method of presenting the cyclic life characteristics of a given material is to plot strain range, $\Delta\epsilon$, as a function of cycles to failure, N_f. It was pointed out earlier in the text that a large compressive strain is induced in the cylinder hot-gas wall during the heating phase of the thermal cycle, and conversely, a tensile strain is induced in the hot-gas wall during the chilldown portion of the cycle. The strain range is the absolute sum of the compressive and tensile strains. Although the total strain in the cylinder wall is caused by a combination of thermal and pressure loads, the major portion is thermal strain and is a function of the extremes in hot-gas-side to backside wall temperature, ΔT, that occurs during a thermal cycle, i.e., the higher the ΔT, the higher the strain. This strain range, which is conventionally used to determine life, is related to the maximum ΔT range between the hot-gas-side wall and backside wall during a thermal cycle.

In view of this, the data presented in Fig. 17 was replotted to show the maximum ΔT range as a function of N_f. To get the maximum ΔT range, the hot-gas-side to backside wall temperature difference had to be calculated for each time slice in the thermal cycle. Figure 18 shows a plot of the calculated ΔT for cylinder S/N 40 taken from the data shown in Fig. 14. There is an overshoot and an undershoot in ΔT during the heat-up and chill-down transients. This is caused by the fact that the hot-gas wall is considerably thinner than the thick backside wall and therefore heats up and cools down at a faster rate than the backside wall. The lag in the backside wall temperature causes the overshoot and undershoot in ΔT. It can also be seen in the figure that if the strain range is proportional to ΔT, then the major part of the strain is caused during the heating portion of the cycle.

Figure 19 shows a log-log plot of the maximum ΔT range for each cylinder plotted as a function of N_f. Curve fits of ΔT vs N_f for the OFHC copper and 1/2-hard Amzirc are also shown. Comparing the curve fits on this figure with the curve fits shown on Fig. 17, it can be seen that the slopes are nearly identical, especially for the 1/2-hard Amzirc. Also, the same conclusions drawn from Fig. 17 can be identically drawn from Fig. 19.

To rank the materials investigated in the present work with the ranking presented in Ref. 6, requires comparing the relative number of cycles to fracture at a given strain range. For example, at a 2% strain range, the number of cycles to fracture was 130 for OFHC copper, 930 for NARloy-Z, and 1400 for 1/2-hard Amzirc. Of the three materials, these results indicate that the 1/2-hard Amzirc is the best material for thrust chamber application. In this investigation the materials were compared by plotting the hot-gas-side wall and the hot-gas-side to backside wall temperature difference versus cycles to failure (figs. 17 and 19). Ranking the cyclic life of the three materials based on temperature, it was shown that there was little difference between the OFHC copper and 1/2-hard Amzirc materials and, that the NARloy-Z and aged Amzirc were the best materials.

In conclusion, the cyclic life rankings of the chamber liner materials using the results of this investigation and those of Ref. 7 do not agree with the rankings in Ref. 6 which are based on uniaxial, isothermal strain tests.

Concluding Remarks

Every fatigue failure in this test program was characterized by a thinning of the cooling passage wall, bulging of the wall toward the thrust chamber centerline, and a severely deformed cooling channel cross-sectional geometry. Although the structural analysis and thrust chamber life prediction is not a part of this report, it would appear that any attempt to do a reasonable life prediction analysis would have to account for the cooling channel geometry change, the resulting change in the wall temperature profile, and the change in material properties encountered during the cyclic life of the thrust chamber.

Summary of Results

During a test program to investigate low cycle thermal fatigue, 22 cylindrical test sections of a cylindrical rocket thrust chamber were fabricated and 21 of them were cycled to failure. The cylinder liners were fabricated from three materials: OFHC copper, Amzirc, and NARloy-Z. The cylinders were fabricated by milling cooling channels into the liner and closing out the backside with electrodeposited copper. The tests were conducted at a chamber pressure of 4.14 MN/m^2 (600 psia) using hydrogen-oxygen propellants at an oxidant-fuel ratio of 6.0, which resulted in an average throat heat flux of 54 MW/m^2 (33 $Btu/in^2/sec$). The cylinders were cooled with liquid hydrogen at an average flow rate of 0.91 Kg/sec (2.0 lbm/sec). The following results were obtained:

1. All of the failures, regardless of material, were characterized by a thinning of the cooling channel wall at the centerline and eventual failure by tensile rupture.

2. Cylinders with liners fabricated from 1/2-hard Amzirc showed little improvement in cyclic life when compared with liners fabricated from OFHC copper.

3. Cylinders with liners fabricated from NARloy-Z and aged Amzirc had the best cyclic life characteristics.

4. The cycles to failure data correlated equally well with hot-gas-side wall temperature, or hot-gas-side to backside wall temperature difference.

5. One cylinder having an OFHC copper liner was cycled 2044 times at a steady-state hot-gas-side wall temperature of 514 K (925° R) without failing.

6. The cyclic life rankings of the materials based on temperature do not agree with the published rankings based on uniaxial, isothermal strain tests.

References

1. Goalwin, D. S., "A High-Pressure Regeneratively Cooled Thrust Chamber. Volume 1: Analysis, Test, and Evaluation," Rocketdyne, Canoga Park, Calif., R-7646-1, Aug. 1969 (AFRPL-TR-68-226-Vol-1; AD-504321L).

2. Kaufmann, M., "A High-Pressure, Cooled Thrust Chamber. Volume 2: Design and Manufacturing Report," Messerschmitt-Boelkow-Blohm GmbH, Munich (West Germany), MBB-TR-900, Aug. 1968 (AFRPL-TR-68-226-Vol-2; AD-507172L).

3. Fulton, D., "Investigation of Thermal Fatigue in Non-Tubular Regeneratively Cooled Thrust Chambers. Volume 1," Rockwell International Corp., Canoga Park, Calif., R-9093-Vol-1, May 1973 (AD-760582; AFRPL-TR-73-10-Vol-1).

4. Fulton, D., "Investigation of Thermal Fatigue in Non-Tubular Regeneratively Cooled Thrust Chambers. Volume 2," Rockwell International Corp., Canoga Park, Calif., R-9093-Vol-2, May 1973 (AD-760583; AFRPL-TR-73-10-Vol-2).

5. Brecheisen, A. W., II, "Microstructural Behavior of Copper-Zirconium Alloy Resulting from Rocket Engine Imposed Thermomechanical Stress." PhD Thesis, Purdue University, Lafayette, Ind., 1975.

6. Conway, J. B., Stentz, R. H. and Berling, J. T., "High Temperature, Low-Cycle Fatigue of Copper-Base Alloys in Argon. Part 1: Preliminary Results for 12 Alloys at 1000° F (538° C)," Mar-Test Inc., Cincinnati, Oh., Aug. 1973; also NASA CR-121259.

7. Tannum, N. P., Kasper, H. J. and Pavli, A. J., "Experimental and Theoretical Investigation of Fatigue Life in Reusable Rocket Thrust Chambers," AIAA Paper 76-685, Palo Alto, Calif., July 1976.

8. Esposito, J. J. and Zabora, R. F., "Thrust Chamber Life Prediction. Volume I: Mechanical and Physical Properties of High Performance Rocket Nozzle Materials," Boeing Aerospace Co., Seattle, Wash., D180-18673-1-Vol-1, Mar. 1975; also NASA CR-134806.

9. Smith, J. P., "Systems Improved Numerical Differencing Analyzer (SINDA): User's Manual," TRW Systems Group, Redondo Beach, Calif., TRW-14690-H001-R0-00, Apr. 1971.

TABLE I. - CYLINDER CONFIGURATIONS AND CYCLES TO FAILURE DATA

Cylinder S/N	Liner material	Length cm (in.)	Cycles to failure N_f
1 N.I.	OFHC Copper	10.16 (4)	817
19			120
22			236
23			150
24			168
33 N.I.		15.24 (6)	220
34			210
35			220
41 N.I.			98
42			56
43			177
*48		10.16 (4)	2044
27	1/2-Hard AMZIRC	10.16 (4)	944
39		15.24 (6)	505
40			381
44			119
45			340
46			106
**56			393
8	NARloy-Z	10.16 (4)	556
9			688
10 N.I.			679

N.I. - Cylinders designated N.I. had no rib or backside thermocouples and the N_f data does not appear in the figures.

* - No failure, stopped testing at 2044 cycles.

** - Cold spun to the 1/2-hard condition and then aged.

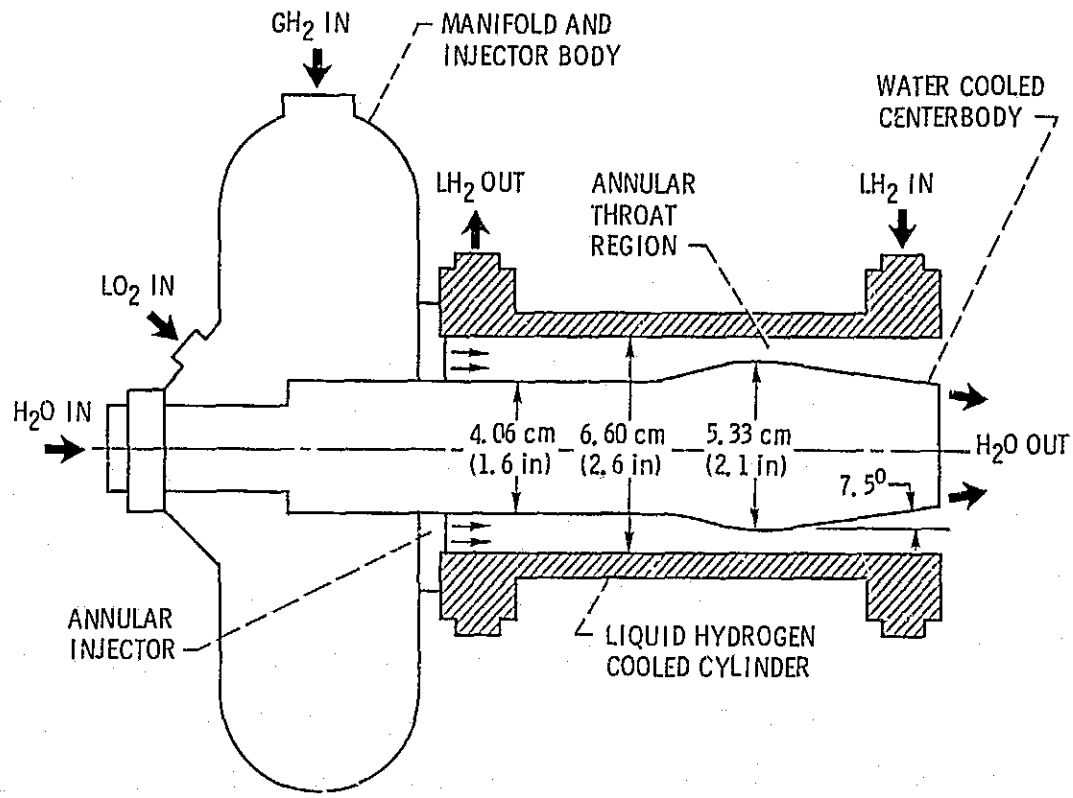

Figure 1. - Schematic of cylindrical thrust chamber assembly.

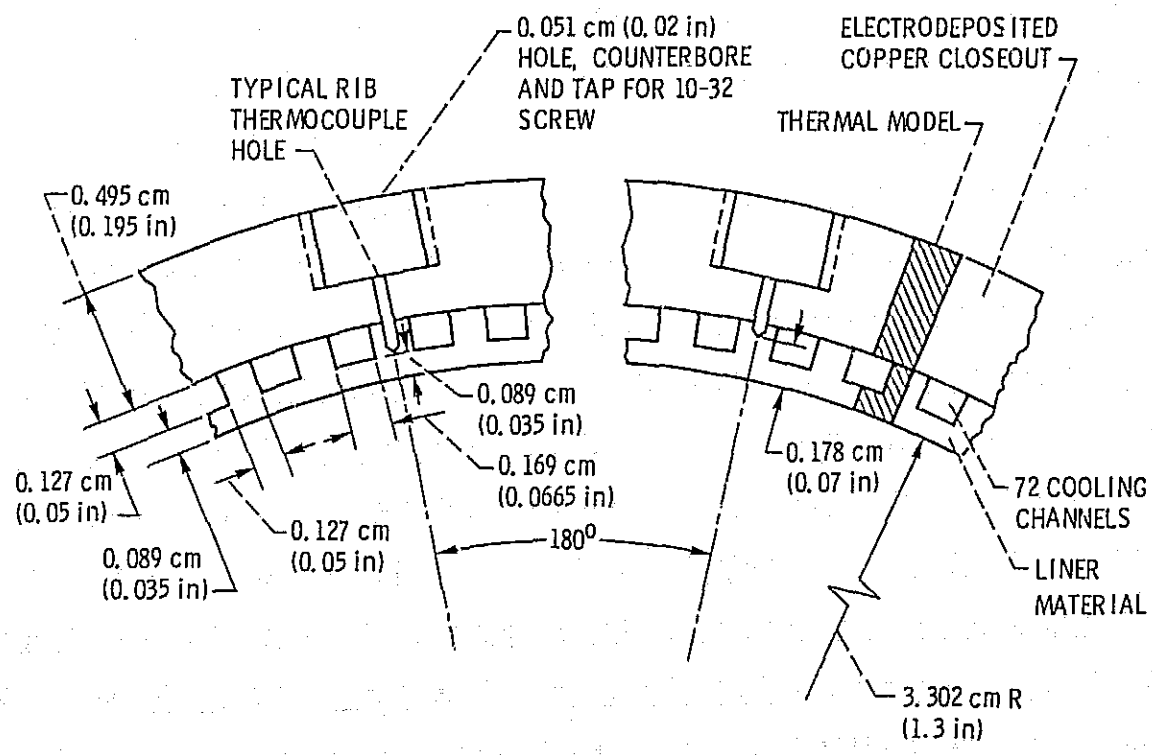

Figure 2. - Cylinder wall cross section showing instrumentation locations and dimensions.

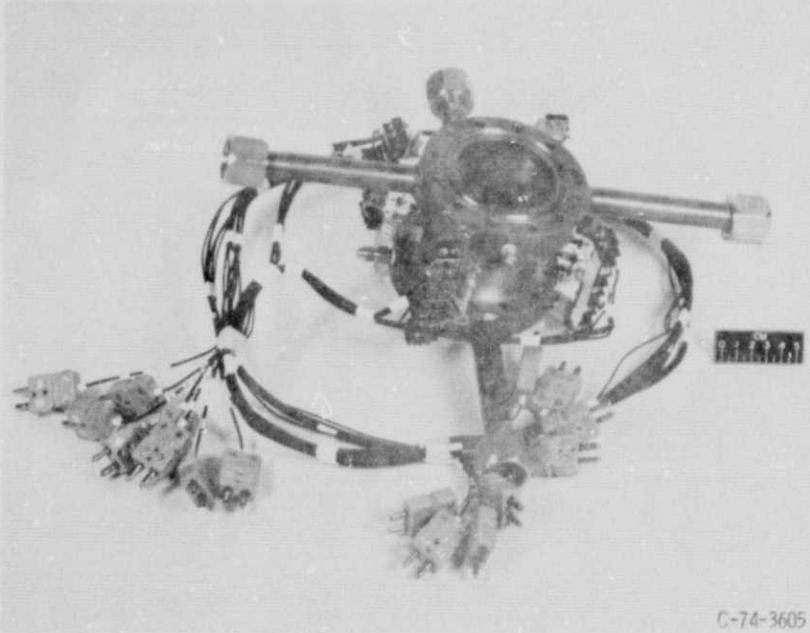

Figure 3. - 10.16 cm (4.0 in.) Cylinder with 12 rib, and 6 backside thermocouples installed. C-76-442

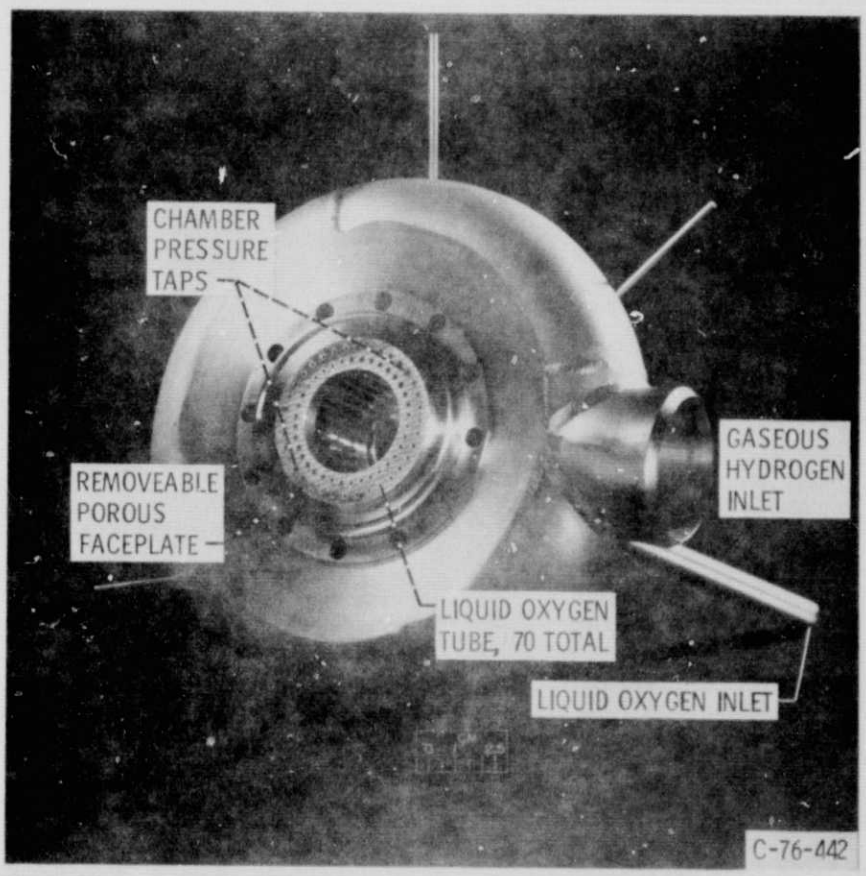

Figure 4. - Annular injector.

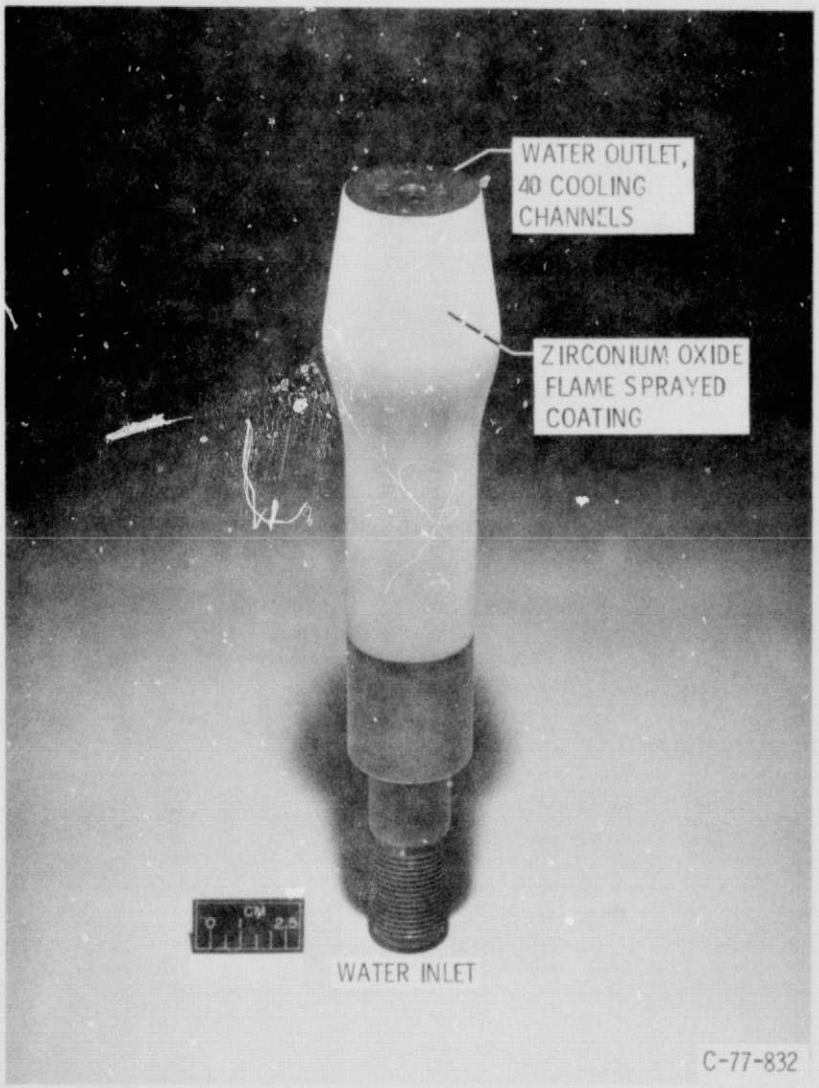

Figure 5. - Ceramic coated, water cooled centerbody for 15.24 cm (6.0 in.) cylindrical thrust chamber.

L_1 THRUST, STRAIN-GAUGE-BRIDGE TYPE LOAD-CELL

F_1, F_2 } OXIDIZER FLOW, TURBINE TYPE FLOW METERS

P_1, P_2 } COMBUSTION CHAMBER PRESSURE, STRAIN-GAUGE-BRIDGE TYPE PRESSURE TRANSDUCER

P_3 OXIDIZER INJECTION PRESSURE, "

P_4 FUEL INJECTION PRESSURE, "

P_5 FUEL ORIFICE PRESSURE "

P_6 COOLANT OUTLET PRESSURE, "

P_7 COOLANT INLET PRESSURE, "

P_8 COOLANT TANK PRESSURE, "

P_9 WATER TANK PRESSURE, "

T_1 OXIDIZER TEMPERATURE AT FLOWMETERS, PLATINUM RESISTANCE BRIDGE TRANSDUCER

T_2 OXIDIZER INJECTION TEMPERATURE, PLATINUM RESISTANCE BRIDGE TRANSDUCER

T_3 FUEL TEMPERATURE AT ORIFICE, COPPER/CONSTANTAN THERMOCOUPLE

T_4 COOLANT TEMPERATURE AT VENTURI, PLATINUM RESISTANCE BRIDGE TRANSDUCER

T_5 COOLANT OUTLET TEMPERATURE, CHROMEL/CONSTANTAN THERMOCOUPLE

T_6 COOLANT INLET TEMPERATURE, PLATINUM RESISTANCE BRIDGE TRANSDUCER

DP_1 OXIDIZER INJECTOR PRESSURE DROP, STRAIN-GAUGE-BRIDGE TYPE PRESSURE TRANSDUCER

DP_2 FUEL INJECTOR PRESSURE DROP, "

DP_3 FUEL ORIFICE PRESSURE DROP, "

DP_4 COOLANT JACKET PRESSURE DROP, "

DP_5 COOLANT VENTURI PRESSURE DROP, "

DP_6 WATER VENTURI PRESSURE DROP, "

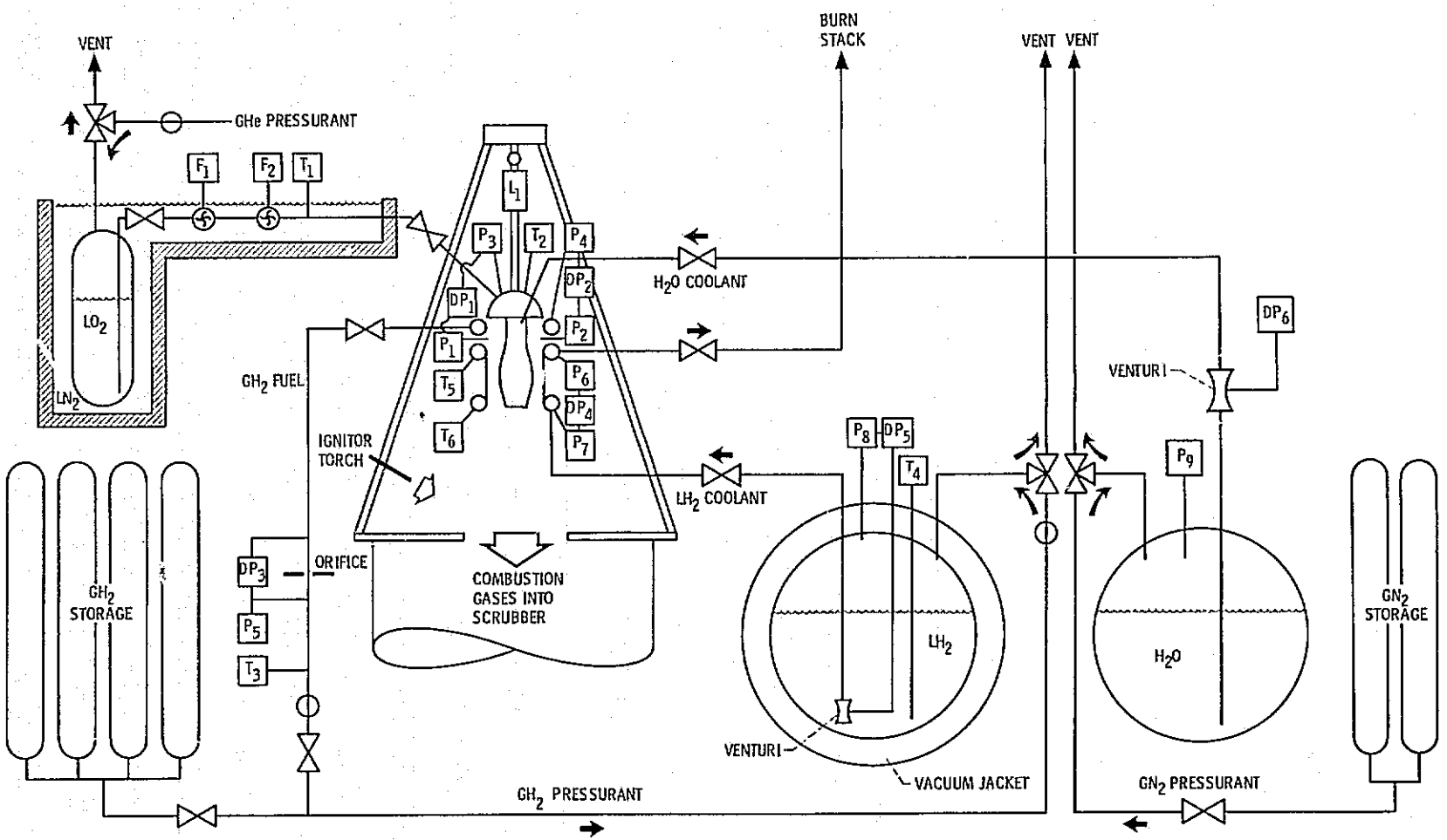

Figure 6. - Schematic of test facility.

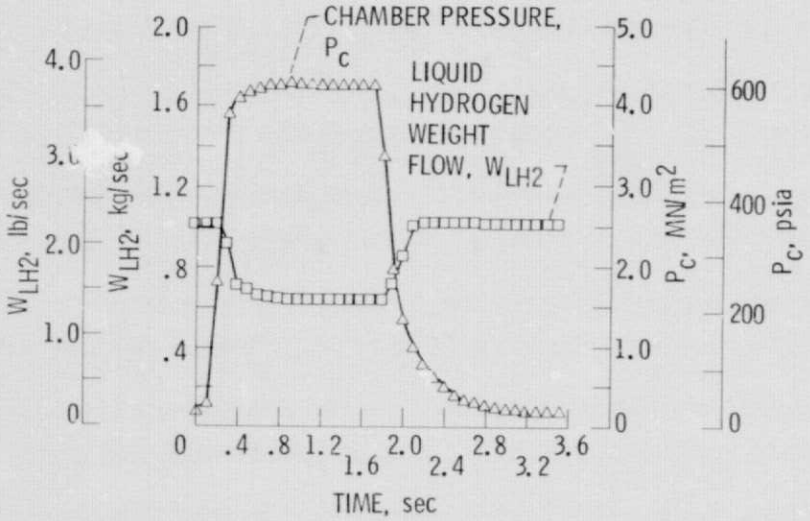

Figure 7. - Computer plot of chamber pressure and liquid hydrogen weight flow for a typical cycle.

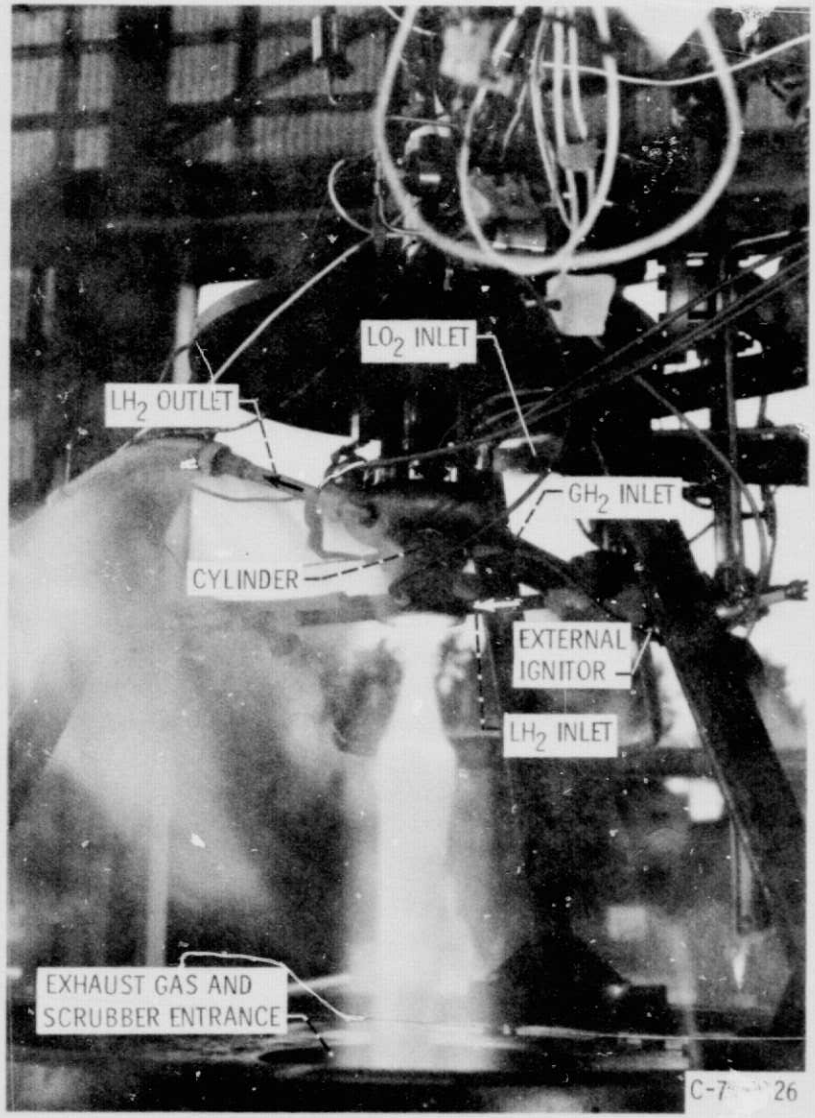

Figure 8. - Cylindrical thrust chamber during cyclic test.

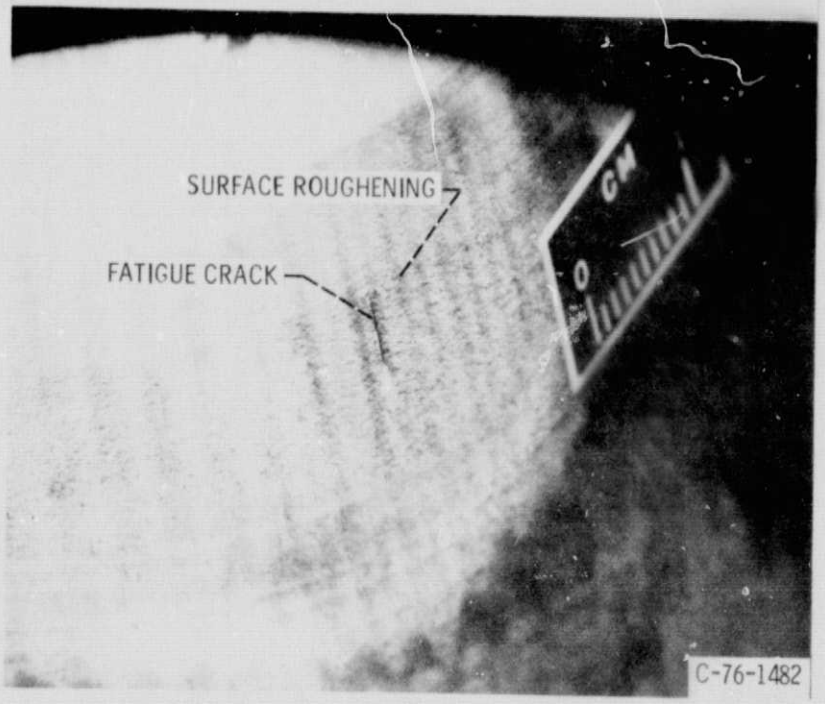

Figure 9. - Fatigue crack in OFHC copper cylinder S/N 33.

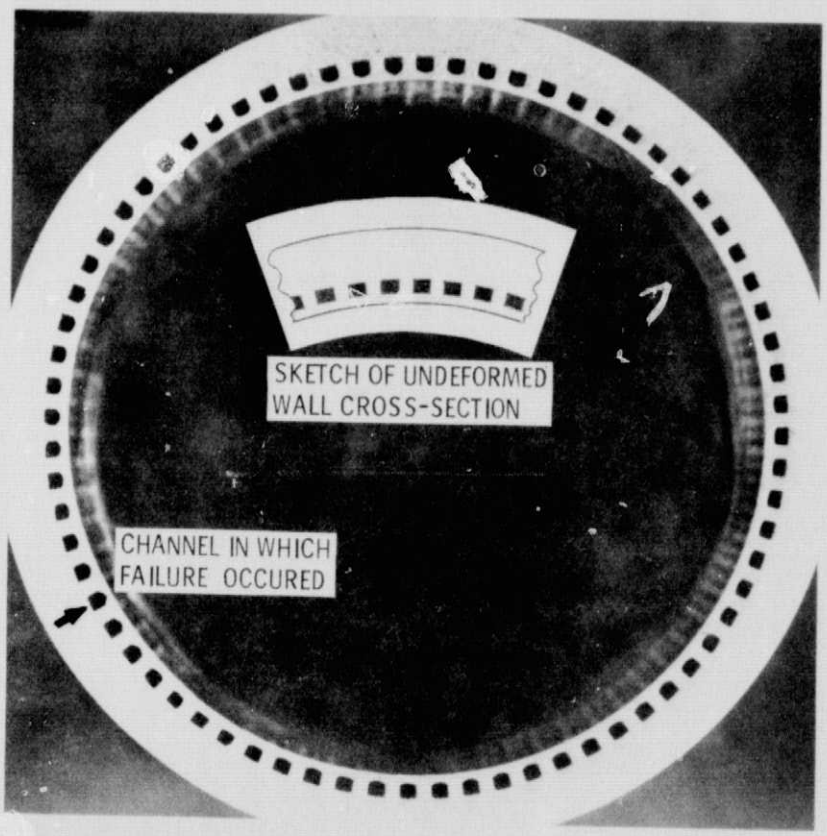

Figure 10. - Cross-section of OFHC copper cylinder S/N 33, 0.152 cm (0.06 in.), downstream of crack location.

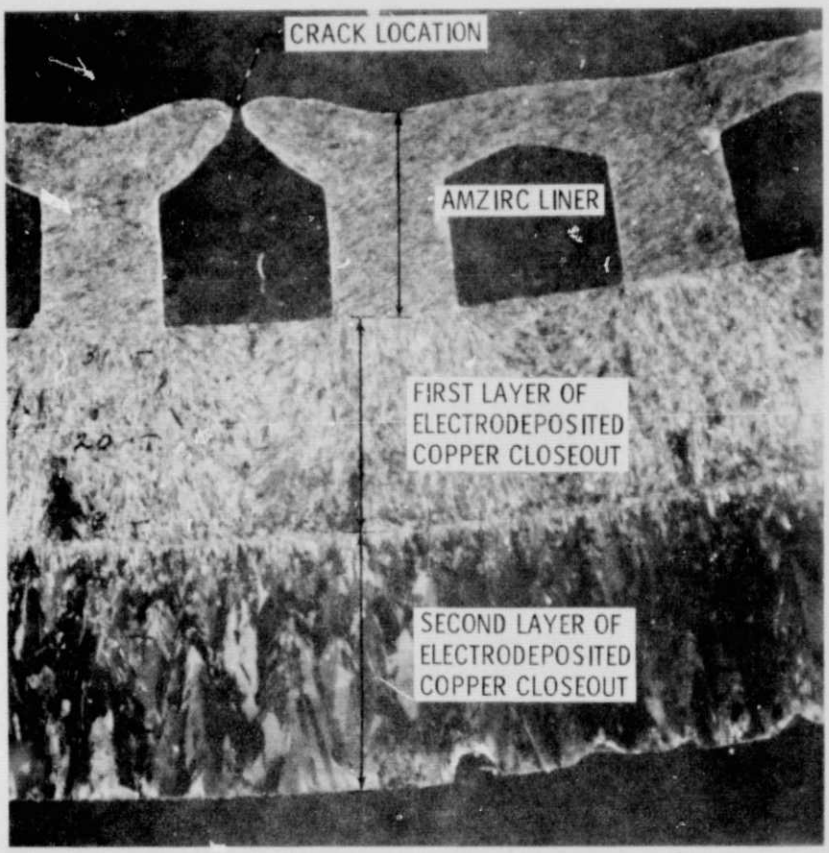

Figure 11. - Cooling channel wall failure in Amzirc cylinder S/N 44.

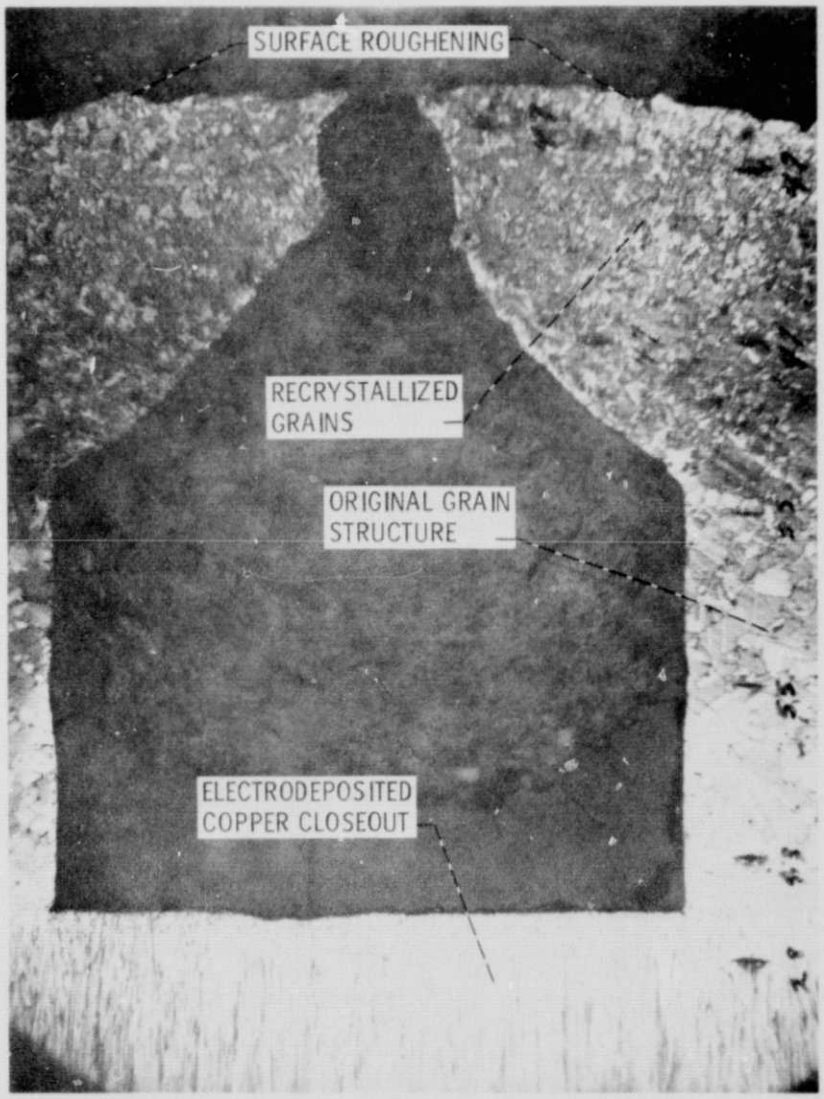

Figure 12. - Cooling channel wall failure in NARloy-Z cylinder S/N 10.

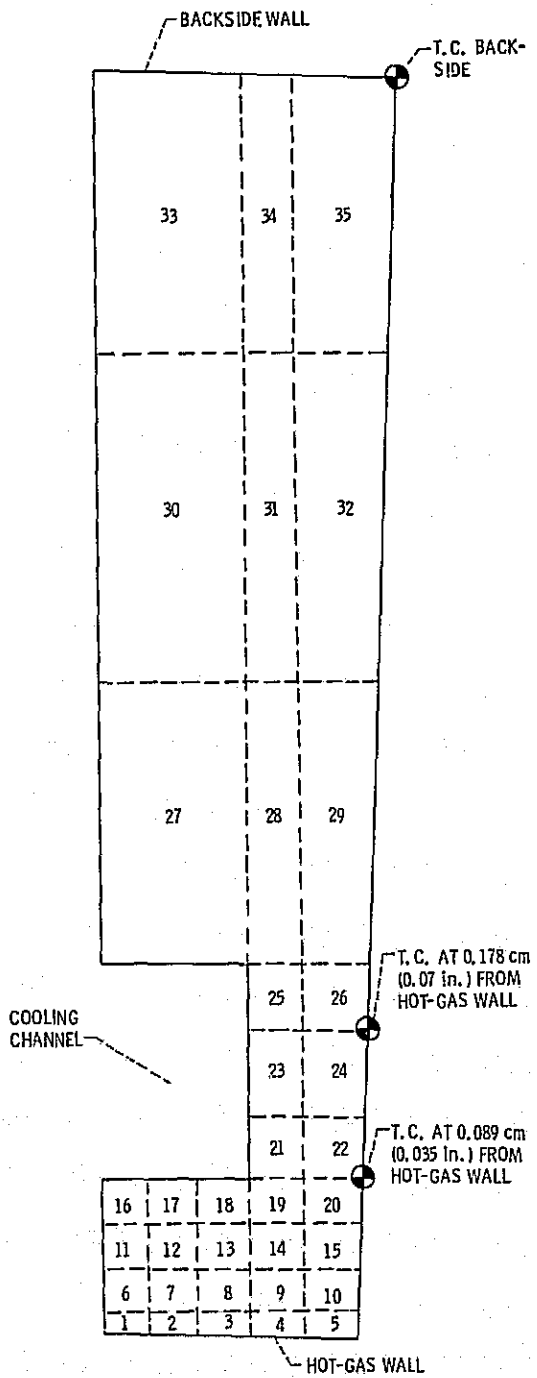

Figure 13. - 35 Element analytical thermal model with the locations of experimental rib and backside temperature measurements superimposed.

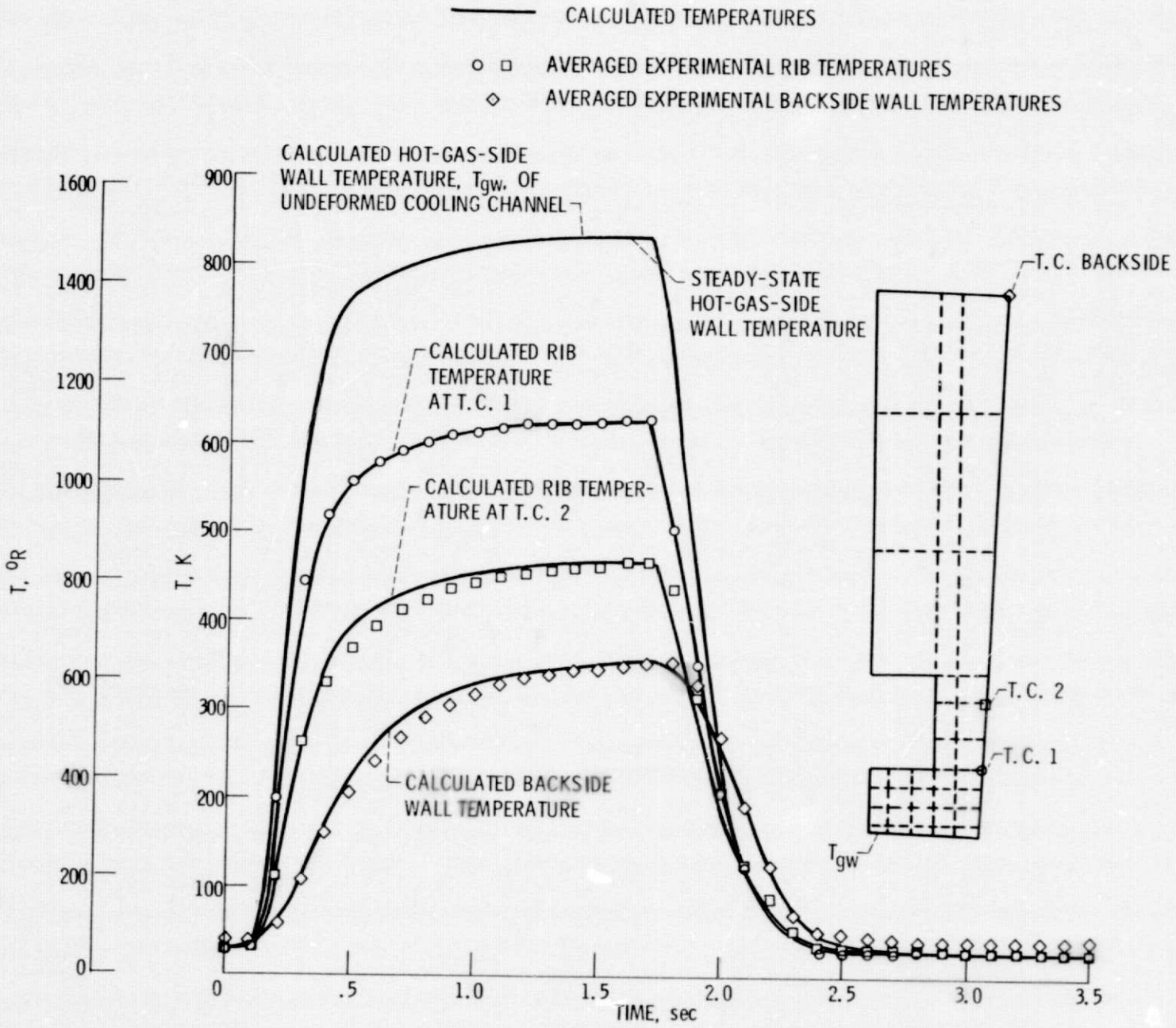

Figure 14. - Matching of thermal analysis with experimental data of 1/2-hard AMZIRC cylinder S/N 40.

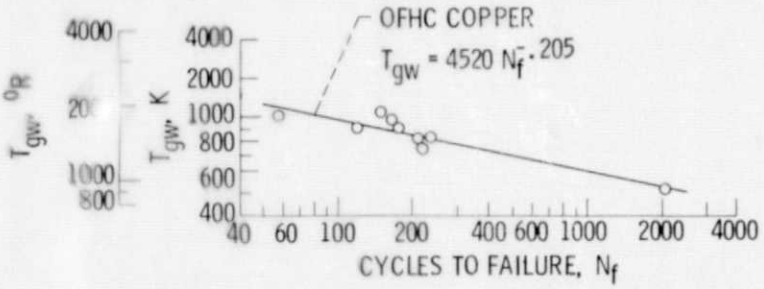

Figure 15. - Calculated steady-state hot-gas-side wall temperature, T_{gw}, versus cycles to failure for the OFHC copper cylinders.

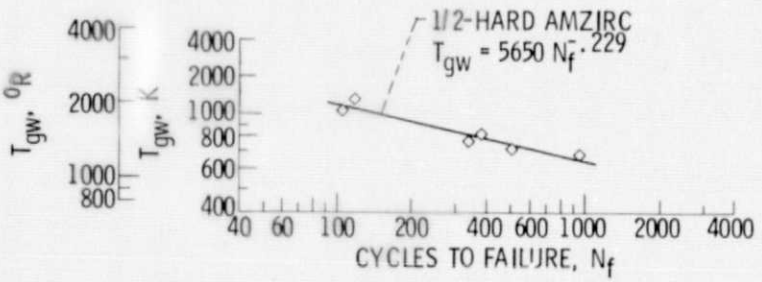

Figure 16. - Calculated steady-state hot-gas-side wall temperature, T_{gw}, versus cycles to failure for the 1/2-hard AMZIRC cylinders.

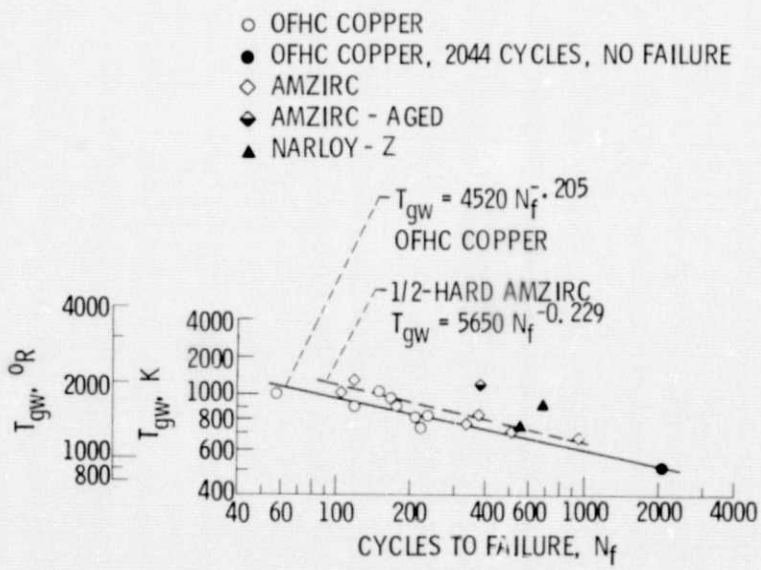

Figure 17. - Calculated steady-state hot-gas-side wall temperature, T_{gw} versus cycles to failure for the OFHC copper, AMZIRC, and NARLOY-Z cylinders.

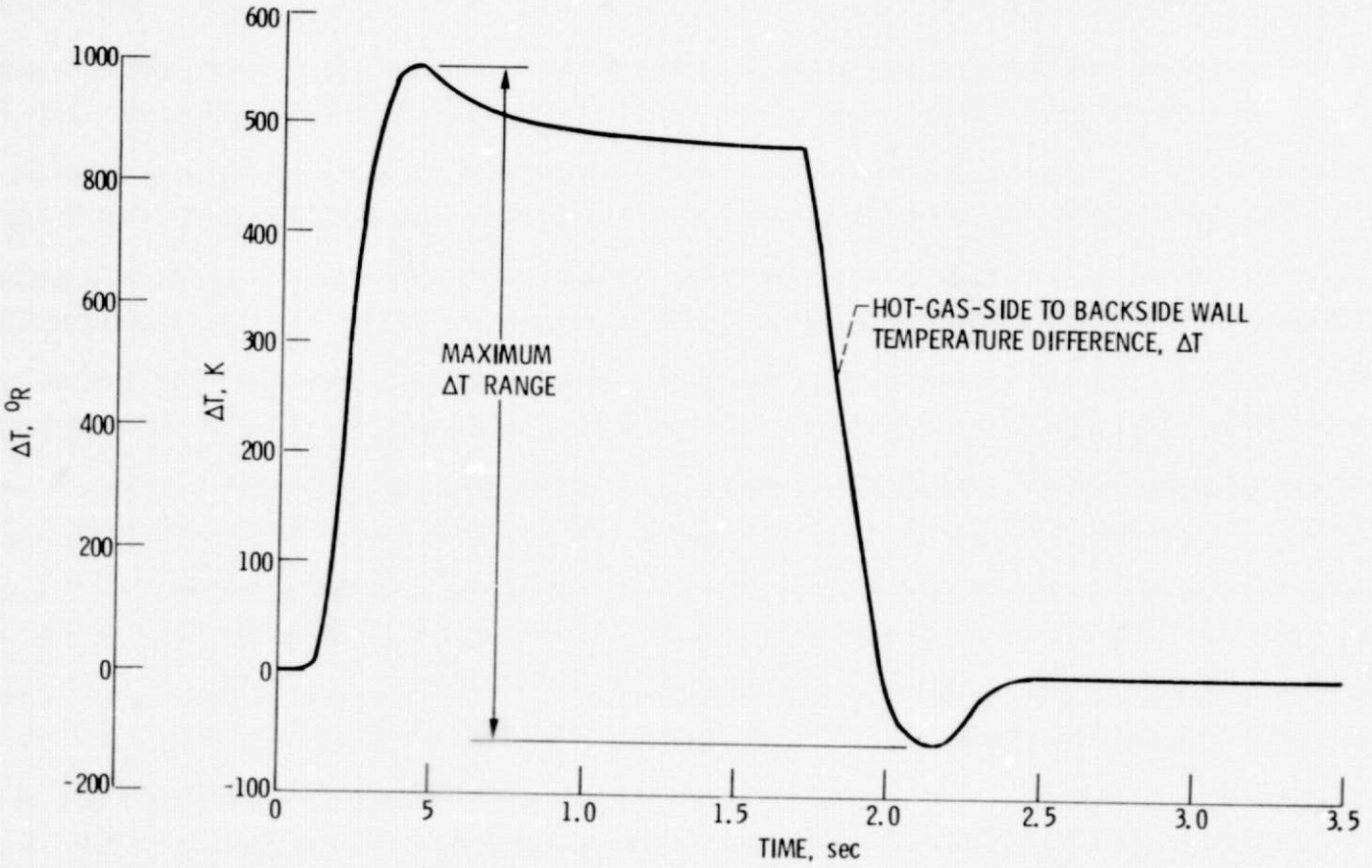

Figure 18. - Calculated hot-gas-side to backside wall temperature difference, ΔT, for 1/2-hard AMZIRC cylinder S/N 40.

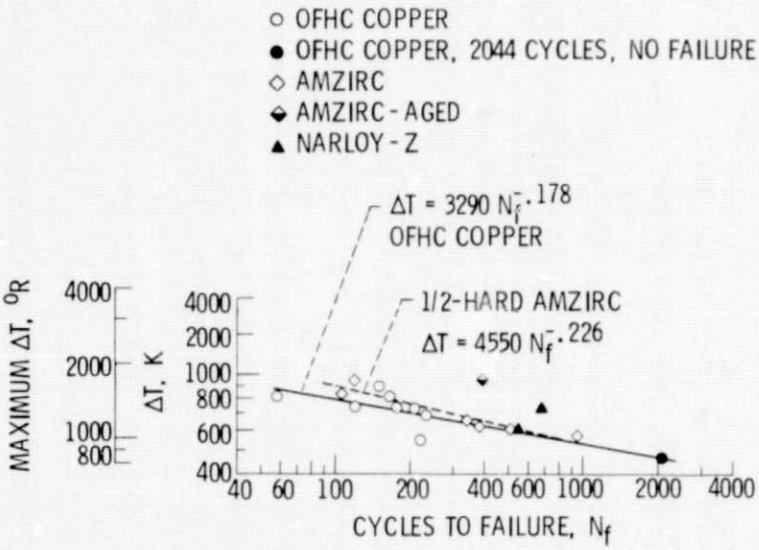

Figure 19. - Maximum hot-gas-side to backside wall temperature difference, ΔT versus cycles to failure for the OFHC copper, AMZIRC, and NARLOY-Z cylinders.